Published in final edited form as:
Biochim Biophys Acta. 2007 October ; 1768(10): 2635–2645.

Oxygen permeability of the lipid bilayer membrane made of calf lens lipids

Justyna Widomska, **Marija Raguz**, and **Witold K. Subczynski***
Department of Biophysics, Medical College of Wisconsin, Milwaukee, Wisconsin 53226, USA

Abstract

The oxygen permeability coefficient across the membrane made of the total lipid extract from the plasma membrane of calf lens was estimated from the profile of the oxygen transport parameter (local oxygen diffusion-concentration product) and compared with those estimated for membranes made of an equimolar 1-palmitoyl-2-oleoylphosphatidylcholine/cholesterol (POPC/Chol) mixture and of pure POPC. Profiles of the oxygen transport parameter were obtained by observing the collision of molecular oxygen with nitroxide radical spin labels placed at different depths in the membrane using the saturation-recovery EPR technique and were published by us earlier (J. Widomska, M. Raguz, J. Dillon, E. R. Gaillard, W. K. Subczynski, Biochim. Biophys. Acta. Epub 2007 March 20). At 35° C, the estimated oxygen permeability coefficients were 51.3, 49.7, and 157.4 cm/s for lens lipid, POPC/Chol, and POPC membranes, respectively (compared with 53.3 cm/s for a water layer with the same thickness as a membrane). Membrane permeability significantly decreases at lower temperatures. In the lens lipid membrane, resistance to the oxygen transport is located in and near the polar headgroup region of the membrane to the depth of the ninth carbon, which is approximately where the steroid-ring structure of cholesterol reaches into the membrane. In the central region of the membrane, oxygen transport is enhanced, significantly exceeding that in bulk water. It is concluded that the high level of cholesterol in lens lipids is responsible for these unique membrane properties.

Keywords

oxygen permeation; lens lipids; lipid bilayer; cholesterol; hydrophobic barrier; membrane rigidity; EPR

1. Introduction

One of the most fundamental properties of biological membranes is that they are barriers to the permeation of polar molecules. This is largely due to the hydrophobicity of the membrane interior. However, this barrier property cannot be automatically extended to the permeation of small solutes such as oxygen, even though some experimental data suggest this to be true [1–7]. The overall conclusion from recent studies of oxygen transport across model and cell plasma membranes is that membranes are not barriers to oxygen transport into the cell and mitochondrion, and created oxygen concentration differences across these membranes at physiological conditions are negligible (see Review [8] and references therein). Only in membranes that contain a high cholesterol concentration and are dense with integral membrane

*CORRESPONDING AUTHOR: Witold K. Subczynski, Department of Biophysics, Medical College of Wisconsin, 8701 Watertown Plank Road, Milwaukee, WI 53226, USA, Tel: (414) 456 4038, Fax: (414) 456 6512, E-mail: subczyn@mcw.edu.

proteins are lipids packed so closely that the solubility and diffusion of oxygen are severely reduced [9–12]. These features are characteristic of the fiber cell plasma membrane of the eye lens, which shows extremely high cholesterol content [13–19] and a high protein-to-lipid ratio [19–22]. These characteristics suggest that the fiber cell plasma membrane can be a moderate barrier to oxygen transport. Additionally, oxygen, on its way to the center of the lens, has to cross many thousands of fiber cell plasma membranes; even a very small oxygen concentration difference across one membrane can, as a result, significantly contribute to the oxygen concentration gradient across the eye lens.

To prevent excessive light scattering and compromised lens transparency, fiber cells lose all subcellular organelles (including mitochondria) during maturation. In fact, the plasma membrane becomes essentially the only supramolecular structure of the matured fiber cells [23]. The plasma membrane of the fiber cell has unique biochemical characteristics, with an extremely high cholesterol level [13,14,18] and a high sphingomyelin content [15,16,19], but only traces of polyunsaturated fatty acids [24,25]. This composition ensures a physical (rigidity [26,27]) and a chemical (resistance to peroxidation [28]) membrane stability. It also allows us to infer that the fiber cell plasma membrane can be a moderate barrier to oxygen transport.

New fiber cells are continuously produced from the epithelial monolayer, and, as a result the adult lens contains two kinds of fiber cells: those located in the lens core, which are maturate and do not contain organelles, and those located in the lens outer layers, which are not yet maturate and contain organelles (including mitochondria). Mitochondrial respiration accounts for approximately 90% of oxygen consumption by the lens [29], which suggests that the outer layers of the fiber cells can be responsible for low oxygen concentration in the lens nucleus.

It is important to note that oxygen concentration in the lens is very low, reaching a value close to zero in the lens core [30,31]. It also has to be mentioned that already at the lens surface the oxygen concentration is low; values of oxygen partial pressure from 2–3 mmHg to 38 mmHg are reported in several vertebrate species [32–38]. An increase in oxygen concentration is thought to be responsible for cataract formation following hyperbaric oxygen treatment or vitrectomy [39–42]. Thus, the knowledge of oxygen concentration and distribution within the lens is of considerable interest. Few polarographic and optode measurements report oxygen partial pressure from 1 mmHg in the cat lens posterior cortex and nucleus [43] to 10–22 mmHg in the rabbit lens [37] and 0.8–4.0 mmHg in the human anterior cortex [44]. These data indicate that to protect against age-related nuclear cataract formation, oxygen concentration in the lens has to be maintained at a very low level.

Because oxygen is constantly consumed, and oxygen consumption reactions are located inside the eye lens [29], it follows that there must be a gradient in oxygen concentration across the fiber cell layers that build the eye lens. Oxygen consumption is necessary to maintain the low oxygen concentration inside the eye lens; otherwise, the concentration of oxygen should be equal to that outside the lens. The value of the oxygen concentration difference across each fiber cell layer is determined by the rate of oxygen consumption by cells confined inside this concentric fiber cell layer and the oxygen permeability coefficient of the cell layer, which is the sum of the permeability coefficient across a cytoplasm and across two plasma membranes. Profiles of the oxygen partial pressure across the isolated bovine lens were reported in an excellent paper by McNulty et al. [29]. They assume, based on the value of the oxygen diffusion coefficient in plasma membrane from erythrocytes [45], that oxygen crosses cell membranes readily, and that membranes provide essentially no resistance to the diffusion of oxygen, as the membranes are very thin barriers. We would like to contribute to this discussion by providing the values of the oxygen permeability coefficient across the membrane made of the total lipid extract from the plasma membrane of calf (bovine) lens and by evaluating the possible contribution of the fiber cell plasma membrane to the created gradients of oxygen

concentration across the eye lens and to the process of maintaining the oxygen concentration in the eye nucleus at a very low level.

The oxygen permeability coefficient across the membrane can, in principle, be measured directly using stop-flow rapid-mixing apparatus to create an oxygen concentration difference across the membrane. These studies have been criticized because the presence of a thick (~2 μm), unmixed water layer on the membrane surface prevents immediate contact of the oxygenated solution with the membrane [46–48]. In other studies, the oxygen permeability coefficient was calculated using the average (single) value of the oxygen diffusion coefficient and the average (single) value of the oxygen membrane concentration [45,49,50]. It was customary to assume that oxygen dissolves and diffuses in the lipid bilayer in a similar way as in bulk hydrocarbon solvents. For example, the value of oxygen concentration in olive oil obtained by Battino et al. [51] was used to evaluate oxygen transport within and across the lipid bilayer. Similarly, in the oxygen diffusion-consumption model, which describes the profile of the oxygen concentration across the bovine eye lens [29], the average (single) value of the oxygen diffusion coefficient in membranes was used. Direct support for these assumptions, however, is lacking. Moreover, a number of reports have indicated that the oxygen diffusion-concentration product changes significantly from the membrane surface to the membrane center [9,10,11,52,53,54,55,56,57]. Subczynski et al. [9] developed the method for the calculation of the oxygen permeability coefficients across the membrane based on the profiles of the oxygen transport parameter (oxygen diffusion-concentration product) across the lipid bilayer, which can be obtained for membranes equilibrated with nitrogen and an air/nitrogen mixture without the need for creating fast-decaying oxygen concentration gradients. Our earlier papers [9,10,11,58] give a solid base for this procedure.

In the present studies, we use our published earlier data of oxygen transport parameters in the lipid bilayer membrane made of the total lipid extract from the calf lens fiber cells [27] to evaluate the oxygen permeability coefficient across this membrane. To elucidate better the major factors that determine membrane resistance to oxygen transport within and across the lens lipid membrane, we compared results obtained for this membrane with those obtained for membranes made of the equimolar 1-palmitoyl-2-oleoylphosphatidylcholine/cholesterol (POPC/Chol) mixture and of the pure POPC. The spin label oximetry measurement splits the lipid bilayer membrane into three well distinguished regions with different permeability properties. Additionally, the comparisons of the regional membrane oxygen permeability coefficients with that of water indicate which region forms a barrier or a pathway (“hydrophobic channels”) for oxygen transport This paper also establishes a methodological base for further investigations of oxygen transport into the human eye lens.

2. Materials and methods

2.1. Calculation of the membrane oxygen permeability coefficient

Bimolecular collision of molecular oxygen (a fast-relaxing species) and the nitroxide (a slow-relaxing species) induces spin exchange, which leads to a faster spin-lattice relaxation of the nitroxide. This effect is measured using the saturation-recovery electron paramagnetic resonance (EPR) technique. An oxygen transport parameter $W(x)$ was introduced as a conventional quantitative measure of the collision rate between the spin label and molecular oxygen [53]:

$$W(x) = T_1^{-1}(\mathrm{Air}, x) - T_1^{-1}(\mathrm{N_2}, x) \quad (1)$$

$T_1(\mathrm{Air},x)$ and $T_1(\mathrm{N_2},x)$ are spin-lattice relaxation times of nitroxides in samples equilibrated with atmospheric air and nitrogen, respectively. Note that $W(x)$ is normalized to the sample equilibrated with the atmospheric air. $W(x)$ is proportional to the product of the local

translational diffusion coefficient $D(x)$ and the local concentration $C(x)$ of oxygen at a depth x in the membrane (which is in equilibrium with the atmospheric air):

$$W(x) = AD(x)C(x) \quad A = 8\pi p r_0 \tag{2}$$

where r_0 is the interaction distance between oxygen and the nitroxide radical spin-label (about 4.5 Å) [52] and p is the probability that an observable event occurs when a collision does occur and is very close to 1 [59,60,61]. A is remarkably independent of the solvent viscosity, hydrophobicity, temperature, and spin label species [59,60,61]. The membrane profiles of $W(x)$ were constructed on the basis of measurements with different lipid spin labels.

Knowledge of the profiles of the oxygen diffusion-concentration product (oxygen transport parameter) makes it possible to calculate a significant membrane characteristic, namely, the oxygen permeability coefficient across the membrane, P_M, which connects the oxygen flux, J, across the lipid bilayer with the difference in oxygen concentration in water on either side of the bilayer ($C'_W - C''_W$):

$$J = -P_M(C'_W - C''_W) \tag{3}$$

The method of calculation for P_M is based on the procedure developed by Subczynski et al. [9]. It is necessary to make an integration of $(D(x)C(x))^{-1}$, which is a measure of the resistance to oxygen permeation, across the entire thickness, h, of the membrane. The product $D(x)C(x)$ can be related to the oxygen transport parameter through the Eq. (2) giving the final equation:

$$P_M(EPR) = \frac{1}{AC_W(air)}\left[\int_0^h \frac{dx}{W(x)}\right]^{-1} \tag{4}$$

Here, $C_W(air)$ is the oxygen concentration in water that is in equilibrium with atmospheric air at the given temperature. $P_M(EPR)$ indicates that measurements were performed using EPR technique.

The oxygen permeability coefficient across the water layer of the same thickness as the membrane, P_W, can also be obtained using the same EPR technique by measuring the oxygen transport parameter in water, $W(water)$, for water soluble spin labels.

$$P_W(EPR) = \frac{1}{AC_W(air)}\left[\int_0^h \frac{dx}{W(water)}\right]^{-1} = \frac{1}{AC_W(air)}\left[\frac{h}{W(water)}\right]^{-1} \tag{5}$$

The $P_M(EPR)$ values were evaluated with the integration performed based on Fig. 1A, where $W(x)^{-1}$ is plotted as a function of distance from the membrane center. The method to obtain $P_W(EPR)$ is illustrated in Fig. 1B. The ratio of $P_M(EPR)/P_W(EPR)$ is the ratio of these two integrals (dashed area in Fig. 1B/dashed area in Fig. 1A).

P_W can also be determined from the macroscopic oxygen diffusion coefficient in bulk water, D_W:

$$P_W(\text{bulk water}) = D_W / h \tag{6}$$

Using EPR measurements in membranes and water, we determined the ratio $P_M(EPR)/P_W(EPR)$, and using the value $P_W(\text{bulk water})$ obtained from Eq. 6, we arrived at a value for the oxygen permeability coefficient across the membrane, P_M.

$$P_M = \frac{P_M(EPR)}{P_W(EPR)} P_W(\text{bulk water}) \tag{7}$$

By taking ratios of P_M(EPR)/P_W(EPR) as determined by the same EPR method, the effect of uncertainty of pr_0 (A in Eqs. 4 and 5) can be reduced.

All calculations of the oxygen permeability coefficients across the membrane were performed based on the profiles of the oxygen transport parameter (oxygen diffusion-concentration product) across membranes made of the total lipid extract from fiber cell plasma membranes of a calf eye lens (lipid extracts from ca. 50 eye lenses were pooled together), the equimolar binary mixture of 1-palmitoyl-2-oleoylphosphatidylcholine/cholesterol (POPC/Chol), and the pure POPC published by us earlier [27,57]. The details connected with sample preparation, saturation-recovery EPR measurements, and processing saturation-recovery date to obtain profiles of the oxygen transport parameter can be found in [27].

In the medical literature, values of oxygen tension in different parts of the body are reported. Oxygen tension is used mainly to describe oxygen concentration in systems that are not in equilibrium with gas phase (and usually not in equilibrium at all), like in the human and animal bodies. It describes the local oxygen concentration and is equal to the partial pressure of oxygen (the same units, torr or mm Hg), which, for a system in equilibrium, will give the same local oxygen concentration. For simplicity, in our calculations and discussion, we use values of oxygen concentration. Oxygen concentration, partial pressure of oxygen, and oxygen tension are mutually related values that, in principle, can be derived from one another. Oxygen concentration in the eye lens can be evaluated from the measured values of oxygen partial pressure by assuming a comparable solubility of oxygen in the lens to that in serum [73], pure water [74], or tumor tissue [75]. For further discussion, see paragraph 2.4, Ref. [8].

3. Results and discussion

3.1. Oxygen permeability across the lens lipid membrane

In Fig. 2, $W(x)^{-1}$, which is a measure of resistance to oxygen permeation, is plotted as a function of the distance from the membrane center in three investigated membranes. $W(x)$ values were taken from the profiles of the oxygen transport parameter presented earlier (see Fig. 9 in Ref. [27] and Fig. 4 in Ref. [57]). As was indicated in [27], all of the saturation-recovery curves were successfully analyzed as single exponentials. When the single exponential fit is satisfactory, the standard deviation for a single fitting is usually better than ±1%, and the decay time constant can be evaluated with an accuracy smaller than ±3% from the mean value for independent experiments (for samples prepared independently). Due to the lack of other data, we assume that the thickness h of the lipid bilayer made of the total lipid extract from the calf eye lens and the locations of nitroxide moieties of the lipid spin labels are the same as those evaluated for the equimolar POPC/Chol mixture. As was explained earlier [27], this model approximates fairly well the fatty acid composition of the calf eye lens membrane. For more details the evaluation of membrane thickness and nitroxide positions, see the explanation in the caption for Fig. 1 and Refs. [9,10].

The oxygen permeability coefficients across the investigated membranes, P_M(EPR), were calculated from profiles of the resistance to oxygen permeation presented in Fig. 2, with the procedure explained in section 2.1. (Eq. 4, with the integration performed based on figures such as Fig. 1A). We evaluated the contribution to the integral from the polar headgroup region by assuming that $W(x)$ through this region is the same as measured with the lipid spin label tempocholine-1-palmitoyl-2-oleoylphosphatidic acid ester (T-PC). It is unlikely that T-PC is monitoring also the hydrophobic region near the membrane surface because the collision of T-PC with the nitroxide at the C5 position cannot be detected by electron-electron double EPR spectrometry [J. B. Feix, unpublished observation]. Profiles across the hydrocarbon region of the bilayer were obtained by connecting all available points with the smooth line. We should mention here the existence of vertical fluctuations of the nitroxide moiety of stearic acid spin

labels toward the polar surface of the lipid bilayers [76,77,78]. From these studies, it can be presumed that distributions of the vertical positions of the nitroxide moiety on n-SASL (n-doxylstearic acid spin label) and n-PC (1-palmitoyl-2-(n-doxylstearoyl)phosphatidylcholine) in the membrane exist, with the mean value of each distribution shifting toward the center as the quantum n increases. Positions of carbon atoms in the alkyl chain were determined by neutron diffraction [62], which showed that the mean positions of these carbons (or free radical moieties attached to those carbons) can be defined with accuracy ±1 Å, even in the liquid-crystalline state. Assuming a Gaussian distribution of the labeled segments in the projection on the bilayer normal, Zaccai et al. [62] report that the time-averaged positional fluctuations increase from 1.5 Å for the C4 position to 3.4 Å for the C12 position. It can be concluded that a nitroxide moiety stays at the position determined by neutron diffraction for most of the time. Based on values of positional fluctuations determined in [62], the upper and lower limit values of P_M(EPR) were also evaluated by assuming maximal displacements of nitroxide positions toward the membrane surface or toward the membrane center. Appropriate profiles that take into consideration these displacements are presented in Fig. 1A, showing that we are evaluating P_M(EPR) with the accuracy ±30%. Thus, the positional fluctuation of the nitroxide is the major source of the uncertainty in evaluating P_M(EPR). This uncertainty is the most prevalent for rectangular oxygen transport parameter profiles (for lens lipid and POPC/Chol membranes), lesser so for bell-shaped profiles (for POPC membranes), and negligible for flat profiles (as for the regional membrane oxygen permeability, see also Section 3.4).

The manner of integration of the oxygen permeability coefficient across a water layer of the same thickness as a membrane (P_W(EPR), Eq. 5) is shown in Fig. 1B. The value of P_W(EPR) can be evaluated with an accuracy smaller than ±3% (the major source of the error is the accuracy of evaluating the oxygen transport parameter). The ratio of P_M(EPR)/P_W(EPR) is the ratio of these two integrals. As previously noted, by using the ratio of P_M(EPR)/P_W(EPR), the effect of uncertainty of A in Eqs. 4 and 5 can be reduced. The final value of P_M was obtained by multiplying P_M(EPR)/P_W(EPR) by the oxygen permeability value through the water layer, P_W(bulk water), as calculated from Eq. 6, using the bulk diffusion coefficients presented in Ref. [79].

Oxygen permeability coefficients for all investigated membranes are presented in Fig. 3 as a function of temperature. At all temperatures (from 15 to 45°C) the oxygen permeability coefficient for the eye lens membrane is practically the same as that for the membrane made of the equimolar POPC/Chol mixture and significantly lower (by factors of 2–3) than that for membranes made of pure POPC. It confirms our earlier statement [27] that the membranes made of the equimolar mixture of POPC/Chol reflect not only the physical properties of the lens lipid membrane but also its permeability properties.

When compared with the oxygen permeability coefficient across a water layer of the same thickness as the membrane, the oxygen permeability coefficient for the lens lipid membrane was found to be smaller only at 15 and 25 °C (2.5 and 1.5 times, respectively). However, this difference practically disappears at 35 °C and at 45 °C the oxygen permeability coefficient for lens lipid membrane became slightly larger than that for a water layer (Fig. 3). Nevertheless, at a temperature lower than 35°C, the lipid bilayer membrane made of the total lipid extract from the eye lens provides a barrier to oxygen transport that is greater than that of a water layer of the same thickness. As can be seen from Fig. 3, this barrier is comparable to that provided by the simple lipid bilayer made of the POPC/Chol mixture and is significantly greater than that provided by the POPC bilayer (without cholesterol).

We would like to indicate here the greater temperature variations for P_M than for P_W (Fig. 3), which is consistent with the results of other investigators. If it is assumed that D(x) and C(x) in Eq. 2 are constants, Eq. 4 becomes $P_M = D_M K_M/h$, where K_M is the oxygen membrane/water

partition coefficient. We also have Eq. 6: $P_W = D_W/h$. Lieb and Stein [80] report that D_M exhibits greater temperature dependence than D_W; both values increase with temperature. In addition, K_M for nonelectrolytes and gases (including oxygen) increases with temperature [81–85]. Because of these dependences, the difference in oxygen permeation between water and membrane, which is significant at a low temperature, becomes quickly less significant with the increase of temperature. We would like to mention here that our evaluations were made for simple lipid bilayer membranes in which the effect of membrane integral proteins was not included. We will return to these problems in section 4.

3.2. Location of the resistance to oxygen permeation

As shown in Fig. 2, in both the eye lens membrane and the POPC/Chol membrane, a rather high permeability barrier for oxygen transport is located in the polar headgroup region and in the hydrocarbon region to the depth of the ninth carbon, which is approximately where the rigid steroid-ring structure of cholesterol reaches into the membrane [68]. The resistance to oxygen permeation in this region is much higher than the resistance in water phase indicated in Fig. 2 by the broken line. However, resistance to oxygen permeation in the membrane center decreases by factors of 3–5 and becomes much less than the resistance to oxygen permeation in the water phase. In the lipid bilayer made of pure POPC, the resistance to oxygen permeation is less than that in the water phase at all locations in the membrane. Surprisingly, the resistance to oxygen permeation in the central region of all three investigated membranes is practically the same and much less than that in water. These data suggest that the high cholesterol content in lens lipid and POPC/Chol membranes is responsible for their low oxygen permeability coefficients by creating the high resistance to oxygen permeation in and near the polar headgroup region. Oxygen transport in the center of the bilayer is practically unaffected by the presence of cholesterol (see profiles of the resistance to oxygen permeation presented in Fig. 2 and profiles of the oxygen transport parameter presented in [27, Fig. 9] and in [60, Fig. 4]).

3.3. Rigidity and hydrophobicity barrier

The lipid bilayer represents the fundamental permeability barrier to the passage of polar molecules into and out of a cell due to its high hydrophobicity. Here we compared the profile of the hydrophobic barrier with the profile of the oxygen transport parameter, both obtained for the lens lipid membrane (Fig. 4). In Fig. 4, we also included appropriate profiles obtained for a pure POPC membrane. These detailed profiles may provide a basis for understanding lens lipid membrane permeability for both polar and non-polar molecules. These profiles were obtained using a variety of lipid spin labels incorporated in the membrane for probing at specific depth. Data for these lipid spin labels are the averages for two lipid leaflets of the symmetrical bilayer. Our smooth profiles resemble theoretical, sigmoidal polarity and oxygen accessibility profiles, proposed earlier for each lipid leaflet [56].

Permeability coefficients of small nonelectrolytes correlate well with oil/water partition coefficients (Overton's rule [87]). In discussing the mechanism by which small nonelectrolytes permeate model and biological membranes, particular attention has been directed toward 1) the location of the permeation barrier in the lipid bilayer, and 2) the physical nature of the rate-limiting barrier [58,80,88–91]. We have shown that the major resistance to permeation of molecular oxygen across the lens lipid membrane is located in the polar headgroup region and the near-surface region in the hydrocarbon phase to the depth of the ninth carbon. We have also shown that the rectangular hydrophobic barrier of the lens lipid membrane is located in the membrane center at locations deeper than the ninth carbon (see Fig. 4B). These results suggest that the locations of the permeation barriers are different for polar and non-polar molecules: for polar molecules, the major permeation resistance is the *hydrophobic barrier* in the central part of the membrane; while for non-polar molecules the permeation resistance is the *rigidity barrier* near the membrane surface.

Fiber cell plasma membranes are known to contain a large concentration of cholesterol. The present results suggest that cholesterol has some functions specific to these membranes. Since the layers of fiber cells in the eye lens separate the lens interior from the external environment, the membrane barriers must be very high to block nonspecific permeation of small molecules across the membrane into the eye interior. Incorporation of cholesterol into the membrane serves this purpose well because cholesterol simultaneously raises the hydrophobic barrier for polar molecules and increases the rigidity barrier for non-polar molecules. A level of hydrophobicity in the lens lipid membrane center, which is comparable to that of hexane and hexadecane ($\varepsilon = 2–3$), should greatly increase activation energy required for polar and ionic small molecules to pass through the membrane. Thus, the rate-limiting step for permeability of small polar molecules is likely to be the process of crossing the hydrophobic barrier at the membrane center.

In the polar headgroup region and the near-surface region in the hydrocarbon phase of the lens lipid membrane, oxygen transport is suppressed to a level close to that of a gel-phase membrane (see Fig. 4A and Refs. [9,92]). We showed previously that the oxygen transport parameter strongly depends on the rate of *gauche-trans* isomerization of lipid alkyl chains [9,10,11,53]. A model for the mechanism of oxygen transport in the membrane has been proposed in which molecular oxygen enters transient small vacant pockets created by *gauche-trans* isomerization of alkyl chains or by the structural nonconformability of neighboring lipids (mismatch in surface topography of molecules when two molecules are placed side by side in the membrane), and oxygen molecules jump from one pocket to an adjacent one or move along with the movement of the pocket itself [10]. It follows that the alkyl chains and sterol rings are well packed in the near surface region, with few vacant pockets to allow entrance and movement of even small molecules such as molecular oxygen, and/or that *gauche-trans* isomerization in this region is as slow as in the gel-phase membrane. Thus, the rate-limiting step for permeation of small non-polar molecules, including molecular oxygen, is likely to be the process of crossing the rigidity barrier located close to the membrane surface.

3.4. Lens lipid membrane: barrier or pathway for oxygen transport

The profile of the hydrophobic barrier of the lens lipid membrane presented in Fig. 4B has many similarities with the profile of the oxygen transport parameter (the product of local concentration and local diffusion coefficient) presented in Fig. 4A. The increase in oxygen transport parallels the increase in hydrophobicity, i.e., a decrease in water penetration. Therefore, the profile for the transport of small hydrophobic molecules is completely opposite of that for water penetration. We should indicate here that the hydrophobicity in the membrane is largely determined by the extent of water penetration into the membrane [93].

The striking similarity between the profile of the oxygen transport parameter and the profile of hydrophobicity in the lens lipid membrane (see Fig. 4) suggests the possibility of lateral transport of molecular oxygen and other small non-polar molecules along the inner core region of the membrane (parallel to the membrane surface), which is referred to as “hydrophobic channeling.” For example, Skulachev [94] noted the possibility of lateral transport of small hydrophobic molecules along the filamentous extended network of mitochondria.

To better illustrate the phenomenon of hydrophobic channeling, we constructed Fig. 5, in which we displayed the temperature dependence of the oxygen permeability coefficient across the membrane region where the major resistance to oxygen permeation is located (from the membrane surface to the depth of the ninth carbon), and for the membrane center, where oxygen transport is enhanced (between tenth carbons in each leaflet). To compare permeability properties of the certain membrane region with those of water, we displayed these data as a ratio of oxygen permeability across the appropriate membrane region (P'_M(EPR)) to that across the water layer of the same thickness (P'_W(EPR)). We observed that the centers of the

cholesterol-containing membranes (both lens lipid and POPC/Chol membranes) can serve as channels for oxygen transport with much higher oxygen permeability than water. To escape from these channels, oxygen has to cross high barriers with low oxygen permeability existing at both sides of the membrane. In pure POPC membranes, oxygen transport is facilitated in all membrane regions, as compared with oxygen transport in water.

Additionally, the activation energy for oxygen translational diffusion in the lens lipid membrane (and the POPC/Chol membrane) is significantly greater in the region where the rigidity barrier is located than that in the membrane center (see Table 1). It is interesting to note that the activation energy in and near the polar headgroup region (T-PC, 5-, 7-PC, 9-SASL positions) in these two membranes is greater than that in the pure POPC bilayer; while in the membrane center (10-, 12-, 14-, 16-PC positions), the activation energy in lens lipid and POPC/Chol membranes is smaller than that in the pure POPC membrane. This supports our hypothesis that in the lens lipid membrane a high cholesterol content is responsible for creating hydrophobic channels for oxygen transport parallel to the membrane surface, and at the same time a high cholesterol content is responsible for creating the rigidity barrier to oxygen transport across the membrane.

4. Final discussion

The oxygen permeability coefficient across the membrane depends on membrane constituents. As shown here and in earlier papers [9,10], cholesterol at high concentration decreases the value of P_M of model membranes three- to five-fold. It is accepted that cholesterol is especially abundant in the plasma membrane of fiber cells. The survey of the literature ensures that in a calf (bovine) eye the lipid bilayer portion of the fiber cell membrane is saturated with cholesterol and the cholesterol-to-phospholipid mole ratio is close to one [13,14,18,20,21,95,96].

In a human eye, the cholesterol level in fiber cell plasma membranes is extremely high, showing cholesterol-to-phospholipid mole ratios from 1 to 2 in the cortex of the lens, to as high as 3 to 4 in the lens nucleus [13,14], and indicating that during aging the cholesterol-to-phospholipid mole ratio increases [97]. It should be mentioned here that at an elevated concentration, cholesterol forms immiscible cholesterol crystalline domains within the lipid bilayer [98]. These domains were also observed within the plasma membrane of fiber cells from the human eye, where they are essential for normal functioning of the eye and maintaining lens transparency to visible light [99–102]. It should be noted here that in membranes overloaded with cholesterol the remaining phospholipid domain should be saturated with cholesterol (with a cholesterol-to-phospholipid mole ratio close to one) and form a liquid ordered-like phase. Thus, the entire membrane (outside the cholesterol crystalline domain) should be organized as in the raft domain (see Rev. [103]). In the lens nucleus of the human eye, the cholesterol crystalline domain can occupy more than 50% of the surface of the lipid bilayer portion of the fiber cell membrane. Thus, this domain should, to a significant extent, determine membrane permeation property. However, to the best of our knowledge, no data exist on oxygen permeability of cholesterol crystalline domain. We can only infer, based on the close packing of the rigid steroid rings in this bilayer, that this membrane can form a significant barrier to oxygen transport. This, however, has to be proved. The most abundant phospholipid in the human lens is dihydrosphingomyelin (~50%), which only represents ~5% in the calf lens membrane [19,26,104]. The strong cholesterol-sphingolipid interaction, as well as the strong dihydrosphingomyelin-dihydrosphingomyelin interaction [104], should decrease oxygen permeability in the human lens as compared with the calf lens. An even more complex situation should exist in the native human lens where intracellular membrane surface is expected to be associated with α-crystallin, which has been shown to exclude water [105–107]. For these membranes, it is likely that the lipid membrane head group region has less free water *in vivo*

than in model systems *in vitro*. However, we will refrain from further discussion of these complicated systems until we obtain more substantial data about oxygen transport within the membrane in the presence of these new components.

The spin-label oximetry allows evaluation of the oxygen permeability coefficient only in the lipid-bilayer portion of model and biological membranes. Because of this, the overall (average) membrane permeability should be further corrected for the presence of integral membrane proteins. Protein content in the membrane can affect oxygen permeability in two ways. First, integral membrane proteins are practically impermeable to oxygen [108,109]. Because of this property, the oxygen permeability coefficient evaluated for the lipid bilayer portion of the membrane should be decreased by a factor proportional to the surface area of its lipid bilayer portion divided by the surface area of the entire membrane. Second, integral membrane proteins affect the oxygen permeability of the lipid bilayer itself mainly by the presence of the boundary regions around integral proteins and by creating protein-rich domains with trapped lipids [11] and/or cholesterol-rich raft domains stabilized by the presence of clustered proteins [12]. For example, in the reconstituted membranes of dimyristoylphosphatidylcholine (DMPC) and bacteriorhodopsin (BR) with a DMPC/BR mole ratio of 80 (BR molecules are monomers in this membrane), the presence of boundary lipids decreases the P_M value by ~1.5, as compared with the pure DMPC bilayer [11]. P_M in the slow oxygen transport domain, with lipid molecules trapped between aggregates of proteins, is smaller by factors of 3–8 compared with that in the pure phospholipids bilayer [11]. In the cholesterol-rich raft domain of the influenza viral membrane, oxygen transport decreased by a factor of 16 compared to bulk lipids [12]. These studies, however, introduce another level of complication.

The next step in creating a more accurate model of fiber cell plasma membranes is the introduction of integral membrane proteins into membranes made from the lipid extract from the fiber cell membranes. The protein content in the fiber cell plasma membrane is rather high. The values reported in the literature for protein-to-lipid ratio (w/w) lie between 1.9 and 2.9 for normal human lens membranes [22] and ~1.5 for calf lens membranes [20,21]. These values are higher than the typical protein-to-lipid ratios in mammalian cell plasma membranes of 0.4 -1.5 but lower than values of ~3.0 reported for protein-rich membranes (halobacterium purple membrane or mitochondrial inner membrane). It is estimated that in the native lens membrane more than 50% of lipid molecules are in contact with intrinsic proteins, which should significantly decrease the oxygen permeation through the lipid-bilayer portion of the membrane. This discussion allows us to conclude that with all of the corrections mentioned above the oxygen permeability coefficient across the native fiber cell plasma membrane should be significantly lower than our evaluation, which shows the upper limit of this coefficient.

Acknowledgements

This work was supported by grants EY015526, EB002052, and EB001980 of the NIH.

References

1. Nicholson P, Roughton FJW. A theoretical study of the influence of diffusion and chemical reaction velocity on the rate of exchange of carbon monoxide and oxygen between the red blood corpuscle and surrounding fluid. Proc Roy Soc B 1951;138:241–264. [PubMed: 14853968]
2. Holland RA. Kinetics of combination of O_2 and CO with human hemoglobin F in cells and in solution. Respir Physiol 1967;3:307–317. [PubMed: 6083204]
3. Chan HC, Glockner JF, Swartz HM. Oximetry in cells and tissue using a nitroxide-liposome system. Biochim Biophys Acta 1989;1014:141–144. [PubMed: 2554973]
4. Glockner JF, Norby SW, Swartz HM. Simultaneous measurement of intracellular and extracellular oxygen concentration using a nitroxide-liposome system. Magn Reson Med 1993;29:12–18. [PubMed: 8380480]

5. Glockner JF, Swartz HM, Pals MA. Oxygen gradients in CHO cells: Measurement and characterization by electron spin resonance. J Cell Physiol 1989;140:505–511. [PubMed: 2550474]
6. Hu H, Sosnovsky G, Swartz HM. Simultanous measurements of the intra- and extra-cellular oxygen concentration in viable cells. Biochim Biophys Acta 1992;1112:161–166. [PubMed: 1333801]
7. Swartz, HM. Measurements of intracellular concentration of oxygen: experimental results and conceptual implications of an observed gradient between intracellular and extracellular concentrations of oxygen. In: Vaupel, P.; Zander, R.; Burley, DF., editors. Oxygen Transport to Tissue XV, Advances in Experimental Medicine and Biology. 345. Plenum; New York: 1994. p. 799-806.
8. Subczynski, WK.; Swartz, HM. EPR oximetry in biological and model samples. Biological Magnetic Resonance. In: Eaton, SS.; Eaton, GR.; Berliner, LJ., editors. Biomedical EPR – Part A: Free Radicals, Metals, Medicine, and Physiology. 23. Kluwer/Plenum; New York: 2005. p. 229-282.
9. Subczynski WK, Hyde JS, Kusumi A. Oxygen permeability of phosphatidylcholine-cholesterol membranes. Proc Natl Acad Sci USA 1989;86:4474–4478. [PubMed: 2543978]
10. Subczynski WK, Hyde JS, Kusumi A. Effect of alkyl chain unsaturation and cholesterol intercalation on oxygen transport in membranes: a pulse ESR spin labeling study. Biochemistry 1991;30:8578–8590. [PubMed: 1653601]
11. Ashikawa I, Yin JJ, Subczynski WK, Kouyama T, Hyde JS, Kusumi A. Molecular organization and dynamics in bacteriorhodopsin-rich reconstituted membranes: Discrimination of lipid environments by the oxygen transport parameter using a pulse ESR spin-labeling technique. Biochemistry 1994;33:4947–4952. [PubMed: 8161556]
12. Kawasaki K, Yin JJ, Subczynski WK, Hyde JS, Kusumi A. Pulse EPR detection of lipid exchange between protein-rich raft and bulk domains in the membrane: Methodology development and its application to studies of influenza viral membrane. Biophys J 2001;80:738–748. [PubMed: 11159441]
13. Li LK, So L, Spector A. Membrane cholesterol and phospholipids in consecutive concentric sections of human lenses. J Lipid Res 1985;26:600–609. [PubMed: 4020298]
14. Li LK, So L, Spector A. Age-dependent changes in the distribution and concentration of human lens cholesterol and phospholipids. Biochim Biophys Acta 1987;917:112–120. [PubMed: 3790601]
15. Byrdwell WC, Borchman D, Porter RA, Taylor KG, Yappert MC. Separation and characterization of the unknown phospholipids in human lens membranes. Invest Ophthalmol Vis Sci 1994;35:4333–4343. [PubMed: 8002253]
16. Byrdwell WC, Borchman D. Lipid chromatography/mass-spectrometric of sphingomyelin and dihydrosphingomyelin of human lens membranes. Ophthalmic Res 1997;29:191–206. [PubMed: 9261843]
17. Varadaraj K, Kushmerick C, Baldo GJ, Bassnett S, Shiels A, Mathias RT. The Role of MIP in lens fiber cell membrane transport. J Membrane Biol 1999;170:191–203. [PubMed: 10441663]
18. Truscott R. Age-related nuclear cataract: a lens transport problem. Ophthalmic Res 2000;32:185–194. [PubMed: 10971179]
19. Huang L, Grami V, Marrero Y, Tang D, Yappert MC, Rasi V, Borchman D. Human lens phospholipid change with age and cataract. Invest Ophthalmol Vis Sci 2005;46:1682–1689. [PubMed: 15851569]
20. Broekhuyse RM, Kuhlmann ED. Lens membrane I. Composition of urea-treated plasma membranes of calf lens. Exp Eye Res 1974;19:297–302. [PubMed: 4417164]
21. Broekhuyse RM, Kuhlmann ED. Lens membrane IV. Preparative isolation and characterization of membranes and various membrane proteins from calf lens. Exp Eye Res 1978;26:305–320. [PubMed: 416964]
22. Gooden MM, Takemoto LJ, Rintoul DA. Evidence for reduced lipid order in plasma membranes from cataractous human lenses. Curr Eye Res 1983;2:367–375. [PubMed: 7168959]
23. Rafferty, NS. Lens morphology. In: Maisel, H., editor. The Ocular Lens: Structure, Function and Pathology. Marcel Dekker; New York: 1985. p. 1-60.
24. Broekhuyse RM, Soeting WJ. Lipids in tissue of the eye: XV. Essential fatty acids in lens lipids. Exp Eye Res 1976;22:653–657. [PubMed: 776644]
25. Zelenka PS. Phospholipid composition and metabolism in the embryonic chicken lens. Exp Eye Res 1978;26:267–274. [PubMed: 639879]

26. Borchman D, Yappert MC, Afzal M. Lens lipids and maximum lifespan. Exp Eye Res 2004;79:761–768. [PubMed: 15642313]
27. Widomska J, Raguz M, Dillon J, Gaillard ER, Subczynski WK. Physical properties of the lipid bilayer membrane made of calf lens lipids: EPR spin labeling studies. Biochim Biophys Acta 2007;1768:1454–1465. [PubMed: 17451639]
28. Huang L, Estrada R, Yappert MC, Borchman D. Oxidation-induced changes in human lens epithelial cells 1. Phospholipids. Free Radic Biol Med 2006;41:1425–1432. [PubMed: 17023269]
29. McNulty R, Wang H, Mathias RT, Ortwerth BJ, Truscott RJW, Bassnett S. Regulation of tissue oxygen levels in the mammalian lens. J Physiol 2004;559:883–898. [PubMed: 15272034]
30. Eaton JW. Is the lens canned? Free Radic Biol Med 1991;11:207–213. [PubMed: 1937139]
31. Harding, JJ. Biochemistry, epidemiology and pharmacology. Chapman and Hall; London: 1991. Cataract.
32. Jacobi KW, Driest J. Oxygen determinations in the vitreous body of the living eye. Ber Zusammenkunft Dtsch Ophthalmol Ges 1966;67:193–198. [PubMed: 6013937]
33. Briggs, D.; Rodenhauser, JH. Distribution and consumption of oxygen in the vitreous body of cats. In: Kessler, M., editor. Oxygen supply: theoretical and practical aspects of oxygen supply and microcirculation of tissue. University Park Press; Baltimore: 1973. p. 265-269.
34. Ormerod LD, Edelstein MA, Schmidt GJ, Juarez RS, Finegold SM, Smith RE. The intraocular environment and experimental anaerobic bacterial endophthalmitis. Arch Ophthalmol 1987;105:1571–1575. [PubMed: 3499883]
35. Fitch CL, Swedberg SH, Livesey JC. Measurement and manipulation of the partial pressure of oxygen in the rat anterior chamber. Curr Eye Res 2000;20:121–126. [PubMed: 10617913]
36. Bassnett S, McNulty R. The effect of elevated intraocular oxygen on organelle degradation in the embryonic chicken lens. J Exp Biol 2003;206:4353–4361. [PubMed: 14581604]
37. Barbazetto IA, Liang J, Chang S, Zheng L, Spector A, Dillon JP. Oxygen tension in the rabbit lens and vitreous before and after vitrectomy. Exp Eye Res 2004;78:917–924. [PubMed: 15051473]
38. Shui YB, Garcia C, Dattilo LK, Rajagopal R, McMillan S, Mak G, Holekamp NM, Lewis A, Beebe DC. Oxygen distribution in the rabit eye and oxygen consumption by the lens. Invest Ophthalmol Vis Sci 2006;47:1571–1580. [PubMed: 16565394]
39. Palmquist BM, Philipson B, Barr PO. Nuclear cataract and myopia during hyperbaric oxygen therapy. Br J Ophthalmol 1984;68:113–117. [PubMed: 6691953]
40. Chung CP, Hsu SY, Wu WC. Cataract formation after pars plana vitrectomy. Kaohsiung J Med Sci 2001;17:84–89. [PubMed: 11416962]
41. Hsuan JD, Brown NA, Bron AJ, Petel CK, Rosen PH. Posterior subcapsular and nuclear cataract after vitrectomy. J Cataract Refract Surg 2001;27:437–444. [PubMed: 11255058]
42. Holekamp NM, Shui YB, Beebe DC. Vitrectomy surgery increases oxygen exposure to the lens: a possible mechanism for nuclear cataract formation. Am J Ophthalmol 2005;139:302–310. [PubMed: 15733992]
43. Uyama, C. Diffusion model of a cat eye. In: Kessler, M., editor. Oxygen supply: theoretical and practical aspects of oxygen supply and microcirculation of tissue. University Park Press; Baltimore: 1973. p. 64-66.
44. Helbig H, Hinz JP, Kellner U, Foerster MH. Oxygen in the anterior chamber of the human eye. Ger J Ophthalmol 1993;2:161–164. [PubMed: 8334391]
45. Fischkoff S, Vanderkooi JM. Oxygen diffusion in biological and artificial membranes determined by the fluorochrome pyrene. J General Physiol 1975;65:663–676.
46. Coin DT, Olson JS. The rate of oxygen uptake by human red blood cells. J Biol Chem 1979;254:1178–1190. [PubMed: 762123]
47. Huxley VH, Kutchai MJ. The effect of the red cell membrane and a diffusion boundary layer on the rate of oxygen uptake by human erythrocytes. J Physiol 1981;316:75–83. [PubMed: 7320883]
48. Huxley VH, Kutchai MJ. Effects of diffusion boundary layers on the initial uptake of oxygen by red blood cells: theory *vs.* experiments. Microvascular Res 1983;26:89–107.
49. Kimich R, Peters A. Solvation of oxygen in lecithin bilayers. Chem Phys Lipids 1975;14:350–362. [PubMed: 1242112]

50. Peters A, Kimich R. The heterogenious solubility of oxygen in aqueous lecithin dispersion and its relation to chain mobility. NMR relaxation and wide-line study. Biophys Struct Mechanism 1978;4:67–85.
51. Battino R, Evans FD, Danforth WF. Solubility of seven gases in olive oil with reference to theories of transport through the cell membrane. J Am Oil Chemists' Soc 1968;45:830–833.
52. Windrem DA, Plachy WZ. The diffusion-solubility of oxygen in lipid bilayers. Biochim Biophys Acta 1980;600:655–665. [PubMed: 6250601]
53. Kusumi A, Subczynski WK, Hyde JS. Oxygen transport parameter in membranes as deduced by saturation recovery measurements of spin-lattice relaxation times of spin labels. Proc Natl Acad Sci USA 1982;79:1854–1858. [PubMed: 6952236]
54. Smirnov AI, Clarkson RB, Belford RL. EPR linewidth (T_2 method to measure oxygen permeability of phospholipids blayer and its use to study the effect of low ethanol concentration. J Magn Reson B 1996;111:149–157. [PubMed: 8661272]
55. Subczynski WK, Lewis RNAH, McElhaney RN, Hodges RS, Hyde JS, Kusumi A. Molecular organization and dynamics of 1-palmitoyl-2-oleoylphosphatidylcholine bilayers containing a transmembrane α-helical peptide. Biochemistry 1998;37:3156–3164. [PubMed: 9485469]
56. Marsh D. Polarity and penetration profiles in lipid membranes. Proc Natl Acad Sci USA 2001;98:7777–7782. [PubMed: 11438731]
57. Subczynski WK, Pasenkiewicz-Gierula M, McElhaney RN, Hyde JS, Kusumi A. Molecular dynamics of 1-palmitoyl-2-oleoylphosphatidylcholine membranes containing transmembrane α-helical peptides with alternating leucine and alanine residues. Biochemistry 2003;42:3939–3948. [PubMed: 12667085]
58. Subczynski WK, Hopwood LE, Hyde JS. Is the mammalian cell plasma membrane a barrier to oxygen transport? J Gen Physiol 1992;100:69–87. [PubMed: 1324973]
59. Hyde JS, Subczynski WK. Simulation of ESR spectra of the oxygen-sensitive spin-label probe CTPO. J Magn Reson 1984;56:125–130.
60. Subczynski WK, Hyde JS. Diffusion of oxygen in water and hydrocarbons using an electron spin resonance spin-label technique. Biophys J 1984;45:743–748. [PubMed: 6326877]
61. Hyde, JS.; Subczynski, WK. Spin-label oximetry. Biological Magnetic Resonance. In: Berliner, LJ.; Reuben, J., editors. Spin labeling: theory and applications. 8. Plenum; New York: 1989. p. 399-425.
62. Zaccai G, Büldt G, Seelig A, Seelig J. Neutron diffraction studies on phosphatidylcholine model membranes II. Chain conformation and segmental disorder. J Mol Biol 1979;134:693–706. [PubMed: 537075]
63. Janiak MJ, Small DM, Shipley GG. Nature of the thermal pretransition of synthetic phospholipids: dimyristoyl- and dipalmitoyllecithin. Biochemistry 1976;15:4575–4580. [PubMed: 974077]
64. Cornell BA, Separovic F. Membrane thickness and acyl chain length. Biochim Biophys Acta 1983;733:189–193. [PubMed: 6882754]
65. Lis LJ, MacAlister M, Fuller N, Rand RP. Interactions between neutral phospholipids bilayer membranes. Biophys J 1982;37:657–665. [PubMed: 7074191]
66. Kucerka N, Tristram-Nagle S, Nagle JF. Structure of fully hydrated fluid phase lipid bilayers with monosaturated chains. J Membr Biol 2005;208:193–202. [PubMed: 16604469]
67. Pandit SA, Chiu SW, Jakobsson E, Grama A, Scott HL. Cholesterol surrogates: a comparison of cholesterol and 16:0 ceramide in POPC bilayers. Biophys J 2007;92:920–927. [PubMed: 17071659]
68. McIntosh TJ. The effect of cholesterol on the structure of phosphatidylcholine bilayers. Biochim Biophys Acta 1978;513:43–58. [PubMed: 718889]
69. Franks NP, Lieb WR. The structure of lipid bilayers and the effects of general anaesthetics. An x-ray and neutron diffraction study. J Mol Biol 1979;133:469–500. [PubMed: 537057]
70. Nagle JF, Wilkinson DA. Lecithin bilayers. Density measurement and molecular interactions. Biophys J 1978;23:159–175. [PubMed: 687759]
71. Janiak MJ, Small DM, Shipley GG. Temperature and compositional dependence of the structure of hydrated dimyristoyl lecithin. J Biol Chem 1979;254:6068–6078. [PubMed: 447695]
72. Levine YK, Wilkins MHF. Structure of Oriented Lipid Bilayers. Nature New Biol 1971;230:69–72. [PubMed: 5279040]

73. Groebe K, Vaupel P. Evaluation of oxygen diffusion distance in human cancer xenografts using tumor-specific in vivo data: role of various mechanisms in the development of tumor hypoxia. Int J Radiot Oncol Biol Phys 1988;15:691–697.
74. Hitchman, M. Measurements of Dissolved Oxygen. John Wiley and Sons; New York: 1964.
75. Grote J, Susskind R, Vaupel P. Oxygen diffusivity in tumour tissue (DS-carcinosarcoma) under temperature conditions within the rang of 20–40 degrees C. Pflugers Arch 1977;372:37–42. [PubMed: 563582]
76. Merkle H, Subczynski WK, Kusumi A. Dynamic fluorescence quenching studies on lipid mobilities in phosphatidylcholine-cholesterol membranes. Biochim Biophys Acta 1987;897:238–248. [PubMed: 3028480]
77. Yin JJ, Feix JB, Hyde JS. Mapping of collision frequencies for stearic acid spin labels by saturation-recovery electron paramagnetic resonance. Biophys J 1990;58:713–720. [PubMed: 2169919]
78. Yin JJ, Subczynski WK. Effect of lutein and cholesterol on alkyl chain bending in lipid bilayers: a pulse electron paramagnetic resonance spin labeling study. Biophys J 1996;71:832–839. [PubMed: 8842221]
79. StDenis CE, Fell CJ. Diffusivity of oxygen in water. Can J Chem Eng 1971;49:885.
80. Lieb, WR.; Stein, WD. Simple diffusion across the membrane bilayer. In: Stein, WD., editor. Transport and Diffusion across Cell Membranes. Academic Press; Orlando: 1986. p. 69-112.
81. Power GG, Stegall H. Solubility of gases in human red blood cell ghosts. J Appl Physiol 1970;29:145–149. [PubMed: 5428886]
82. Katz Y, Diamond JM. Thermodynamic constants for nonelectrolyte partition between dimyristoyl lecithin abd water. J Membr Biol 1974;17:101–120. [PubMed: 4407659]
83. Dix JA, Kivelson D, Diamond JM. Molecular motion of small nonelectrolyte molecules in lecithine bilayer. J Membr Biol 1978;40:315–342. [PubMed: 209192]
84. Subczynski WK, Hyde JS. Concentration of oxygen in lipid bilayer using a spin-label method. Biophys J 1983;41:283–286. [PubMed: 6301572]
85. Smotkin ES, Moy FT, Plachy WZ. Dioxygen solubility in aqueous phosphatidylcholine dispersion. Biochim Biophys Acta 1991;1061:33–38. [PubMed: 1995055]
86. Subczynski WK, Wisniewska A, Yin JJ, Hyde JS, Kusumi A. Hydrophobic barrier of lipid bilayer membranes formed by reduction of water penetration by alkyl chain unsaturation and cholesterol. Biochemistry 1994;33:7670–7681. [PubMed: 8011634]
87. E. Overton, Ueber die allgemeinen osmotischen Eigenschaften der Zelle, ihre vermutlichen Ursachen und ihre Bedoutung für die Physiologie (Translated by R. B. Park, On the general osmotic properties of the cell, their probable origin, and their significance for physiology in: D. Branton, R. B. Park (Eds.), Papers on Biological membrane Structure, Little, Brown and Co., Boston, 1968), Vierteljahrsschr Naturforsch. Ges., Zürich 44 (1899) 88–135.
88. Diamond JM, Katz Y. Interpretation of nonelectrolyte partition coefficients between dimyristoyl lecithin and water. J Membr Biol 1974;17:121–154. [PubMed: 4407798]
89. Walter A, Gutknecht J. Permeability of small nonelectrolytes through lipid bilayer membranes. J Membr Biol 1986;90:207–217. [PubMed: 3735402]
90. Leahy DE, Wait AR. Solute transport resistance at water-oil interface. J Pharm Sci 1986;75:1157–1161. [PubMed: 3559925]
91. Subczynski, WK.; Hyde, JS. Membranes: barriers or pathways for oxygen transport. In: Hudetz, AG., editor. Oxygen Transport to Tissue XX, Advances in Experimental Medicine and Biology. 345. Plenum; New York: 1998. p. 799-806.
92. Subczynski WK, Wisniewska A, Hyde JS, Kusumi A. Tree-dimensional dynamic structure of the liquid-ordered domain in lipid membranes as examined by pulse-EPR oxygen probing. Biophys J 2007;92:1573–1584. [PubMed: 17142270]
93. Griffith OH, Dehlinger PJ, Van SP. Shape of the hydrophobic barrier of phospholipids bilayers (Evidence for water penetration into biological membranes). J Membr Biol 1974;15:159–192. [PubMed: 4366085]
94. Skulachev VP. Power transmission along biological membranes. J Membr Biol 1990;114:97–112. [PubMed: 2111408]

95. Broekhuyse RM. Membrane lipids and proteins in ageing lens and cataract. Ciba Foundation Symposium 1973;19:135–149.

96. Roy D, Rosenfeld L, Spector A. Lens plasma membrane: isolation and biochemical characterization. Exp Eye Res 1982;35:113–129. [PubMed: 7151881]

97. Truscott RJW. Age-related nuclear cataract: a lens transport problem. Ophthalmic Res 2000;32:185–194. [PubMed: 10971179]

98. Bach D, Wachtel E. Phospholipid/cholesterol model membranes: formation of cholesterol crystallites. Biochim Biophys Acta 2003;1610:187–197. [PubMed: 12648773]

99. Borchman D, Cenedella RJ, Lamba OP. Role of cholesterol in the structural order of lens membrane lipids. Exp Eye Res 1996;62:191–197. [PubMed: 8698079]

100. Jacob RF, Cenedella RJ, Mason RP. Direct evidence for immiscible cholesterol domains in human ocular lens fiber cell plasma membranes. J Biol Chem 1999;274:31613–31618. [PubMed: 10531368]

101. Jacob RF, Cenedella RJ, Mason RP. Evidences for distinct cholesterol domains in fiber cell membranes from cataractous human lenses. J Biol Chem 2001;276:13573–13578. [PubMed: 11278611]

102. Mason RP, Tulenko TN, Jacob RF. Direct evidence for cholesterol crystalline domains in biological membranes: role in human pathobiology. Biochim Biophys Acta 2003;1610:198–207. [PubMed: 12648774]

103. Munro S. Lipid rafts: elusive or illusive. Cell 2003;115:377–388. [PubMed: 14622593]

104. Yappert MC, Borchman D. Sphingolipids in human lens membranes: an update on their composition and possible biological implication. Chem Phys Lipids 2004;129:1–20. [PubMed: 14998723]

105. Borchman D, Tang D. Binding Capacity of -crystallin to bovine lens lipids. Exp Eye Res 1996;63:407–410.α. [PubMed: 8944547]

106. Tang D, Borchman D, Yappert MC. Alpha-Crystallin/lens lipid interactions using resonance energy transfer. Ophthalmic Res 1999;31:452–462. [PubMed: 10474075]

107. -crystallinαGrami V, Marrero Y, Huang L, Tang D, Yappert MC, Borchman D. binding in vitro to lipids from clear human lenses. Exp Eye Res 2005;81:138–146. [PubMed: 15967437]

108. Altenbach C, Greenhalgh DA, Khorana HG, Hubbell WL. A collision gradient method to determine the immersion depth of nitroxides in lipid bilayers: Application to spin-labeled mutants of bacteriorhodopsin. Proc Natl Acad Sci USA 1994;91:1667–1671. [PubMed: 8127863]

109. Subczynski WK, Renk GE, Crouch RK, Hyde JS, Kusumi A. Oxygen diffusion-concentration product in rhodopsin as observed by a pulse ESR spin labeling method. Biophys J 1992;63:573–577. [PubMed: 1330032]

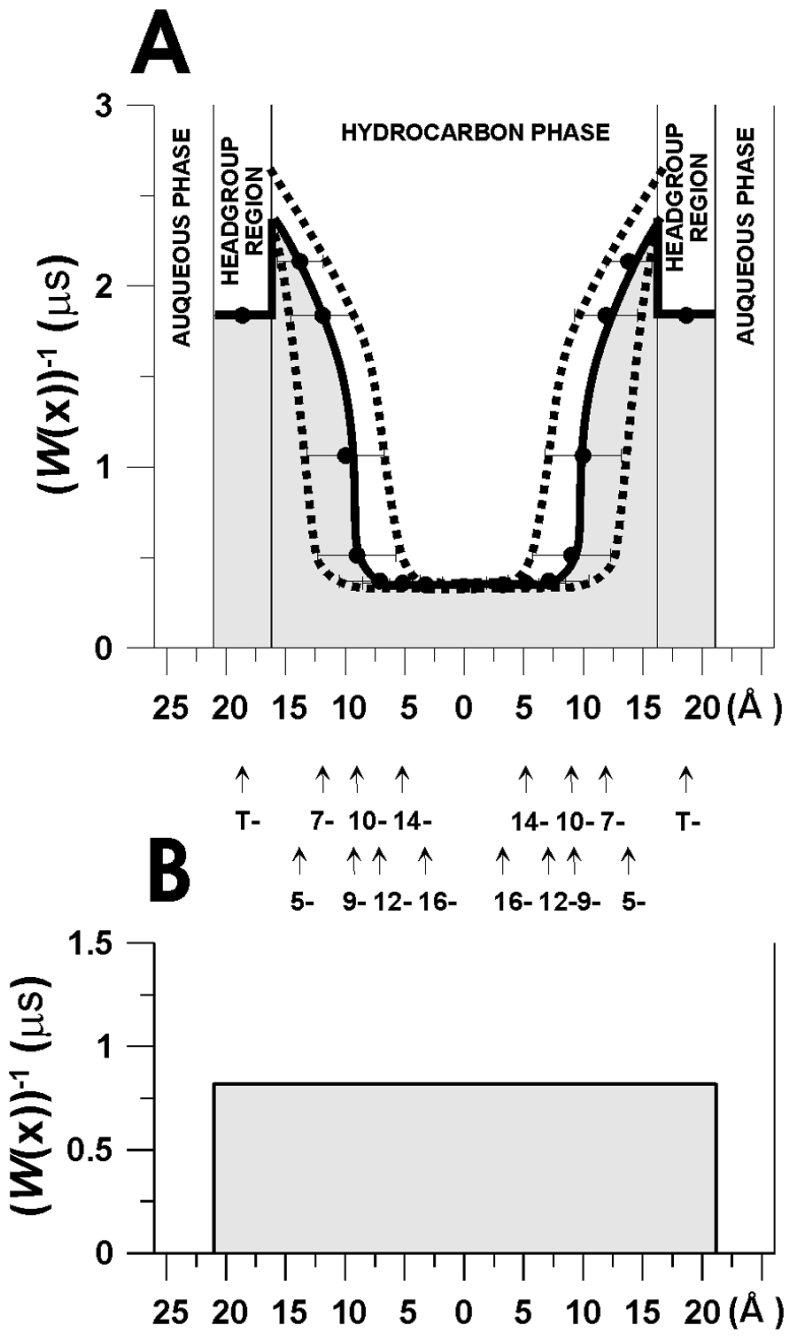

Fig. 1.

The manner of evaluation of the oxygen permeability coefficient across the membrane and across the water layer of the same thickness as the membrane. (A) $W(x)^{-1}$ is plotted as a function of the distance from the center of the lens lipid bilayer at 25°C to show the method of integration for Eq. 4 (i.e., measuring the hatched area under the solid curve). The thickness of the membrane was assumed to be the same as the thickness of the POPC/Chol = 1/1 membrane and was evaluated as described in [9,10]. It is assumed that the location of the alkyl chain carbon atom in the membrane change linearly with the position on the alkyl chain [62,63]. We assume that nitroxide moieties in n-PS and 9-SASL are located at the same depth as appropriate carbon atoms of the 2-chain of POPC. Broken lines show the maximal and minimal evaluations (see

paragraph 3.1 for more details). (B) $W(\text{water})^{-1}$ at 25°C plotted for a water layer of the same thickness as the membrane in order to illustrate the method of integration for Eq. 5 (i.e., measuring the hatched area under the solid line). The thicknesses of the hydrocarbon layer and of the polar headgroup region (including the glycerol ester groups) were calculated for POPC at 0 and 50 mol% cholesterol following procedure similar to those described by Cornell and Separovic [64], from published membrane thickness data for membranes without and with cholesterol [65], the surface area of the POPC in the bilayer [66,67], and the average volume of the POPC molecule as well as CH2, CH3, and CH=CH groups as given in Ref. [66]. Because cholesterol does not affect the thickness of the polar headgroup region [68], its effect on the thickness of the hydrocarbon layer could be estimated from data on the thickness of cholesterol-containing membranes [63,65,69]. The same volumes were used for all temperatures what is justified by the observation that well above the main phase transition temperature the average volumes asymptotically approaches constant, temperature- and chain-length-independent value [63,70,71]. The thickness of POPC at 0 and 50 mol% cholesterol was estimated from membrane thickness of EYPC [65,72]

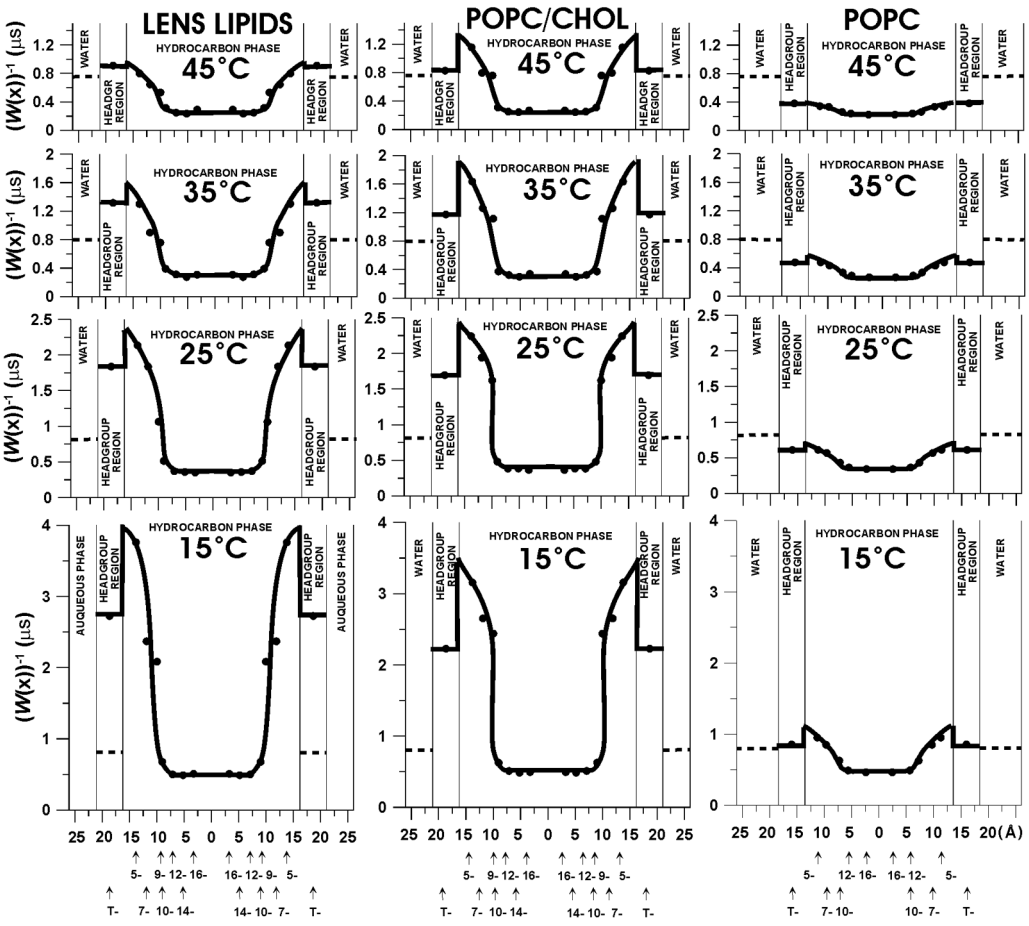

Fig. 2.

$W(x)^{-1}$, which is the measure of the resistance to oxygen permeation, is plotted as a function of the distance from the center of the lens lipid (A), POPC/Chol (B), and pure POPC membranes (C) to show the oxygen permeability barriers. The value of the $W(\text{water})^{-1}$, the resistance to oxygen permeation in aqueous phase, is also indicated as a broken line. It does not change significantly with temperature because temperature dependences of oxygen translational diffusion and oxygen solubility in water are opposite. Again, the oxygen transport parameter is the product of the oxygen concentration and oxygen diffusion coefficient for sample in equilibrium with air at a given temperature.

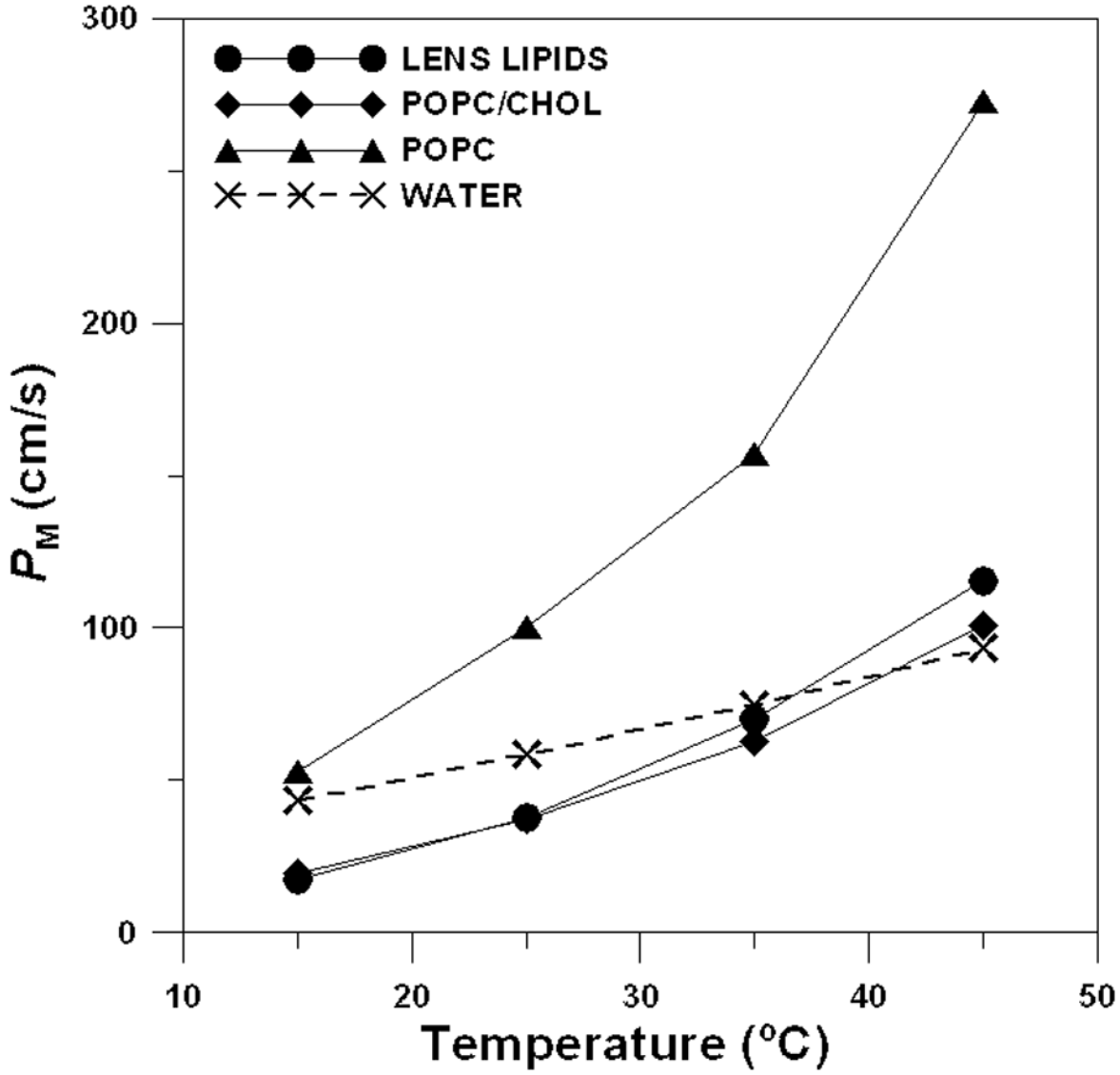

Fig. 3.

Oxygen permeability coefficient across the lens lipid (●), POPC/Chol (◆), and POPC membranes (▲) plotted as a function of temperature. For comparison, the oxygen permeability coefficient across the water layer of the same thickness as the membrane is also indicated as a broken line. P_M values were estimated with the accuracy ≤30% (see Section 3.1 for further explanation).

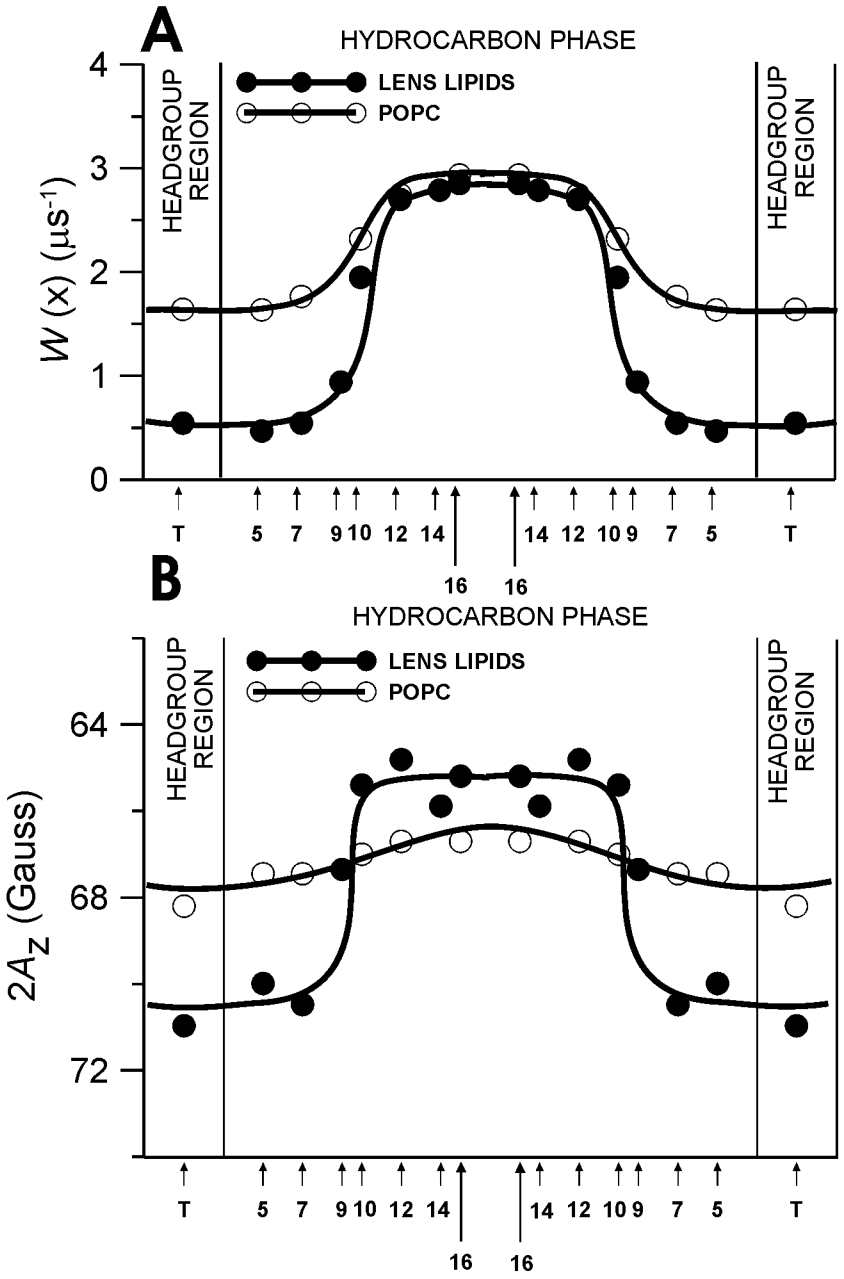

Fig. 4.

Profiles of the oxygen transport parameter (A) and hydrophobicity profiles (B) across the lens lipid membrane (●) are displayed to indicate that the rigidity and hydrophobicity barriers in the lens lipid membrane are located in the different membrane regions. Appropriate profiles across the pure POPC membrane (○) are also added to indicate that the rigidity and hydrophobicity barriers in the lens lipid membrane are created by the high cholesterol content in this membrane. In (A) $W(x)$ is plotted as a function of position in the lipid bilayer (see [27] for more details). In (B), $2A_Z$ (z component of the nitroxide hyperfine interaction measured with the accuracy of ±0.3 G) is plotted as a function of position in the lipid bilayer. Upward changes indicate an increase in hydrophobicity. The A_Z value in the membrane can be related to the local dielectric constant in the membrane (which for brevity is termed “hydrophobicity”)

by referring to Fig. 1 in Ref. [86]. The A_Z value is also correlated with the local concentration of water at a given depth in the membrane, although it does not give an absolute concentration of water. See Ref. [86] for more details.

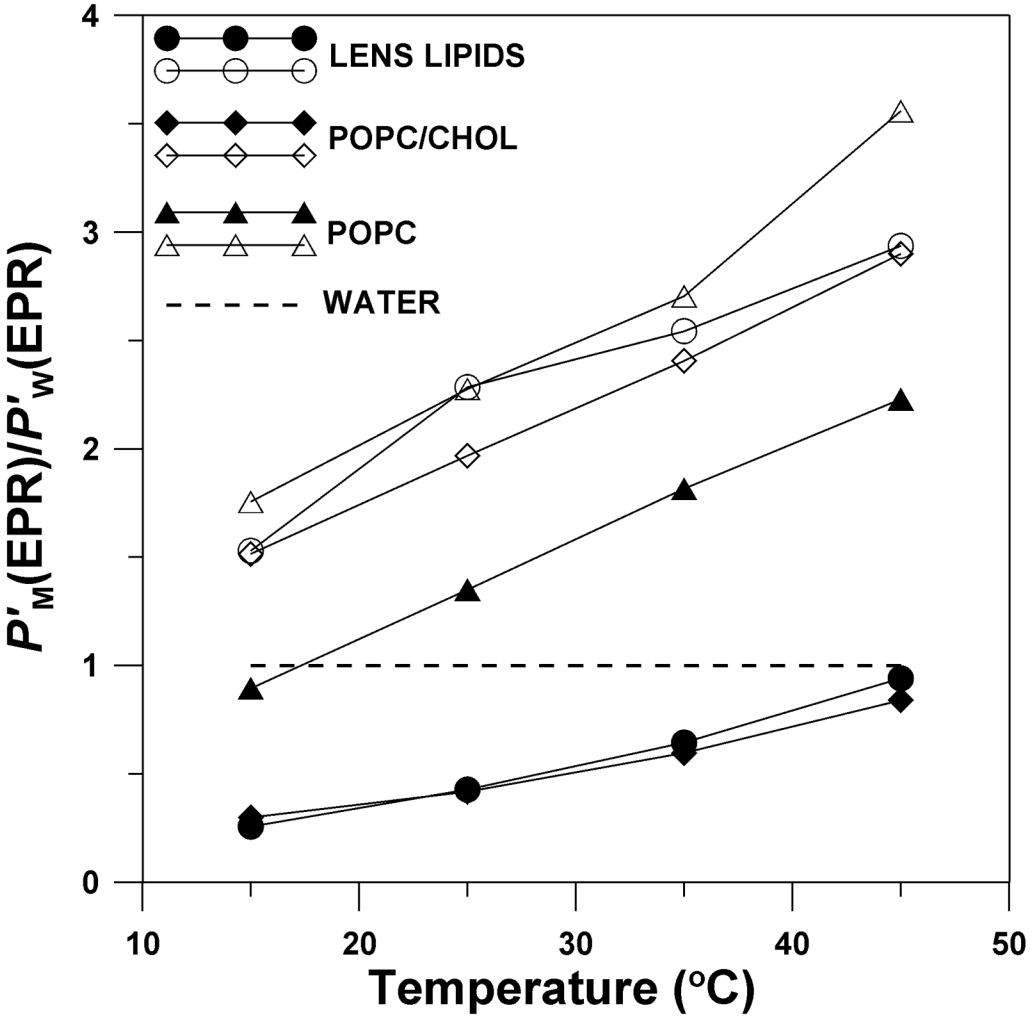

Fig. 5.

Oxygen permeability coefficient across the certain membrane region (P'_M(EPR)) relative to that across a water layer of the same thickness as the membrane region (P'_W(EPR)), i.e., P'_M(EPR)/P'_W(EPR), for lens lipids (●, ○), POPC/Chol (◆, ◇), and pure POPC membranes (▲, Δ) is plotted as a function of temperature. Both P'_M(EPR) and P'_W(EPR) were obtained by theEPR method. Closed symbols (●, ◆, ▲) indicate the membrane region from the membrane surface to the depth of the ninth carbon (measurements with T-PC, 5-, 7-PC, and 9-SASL), and open symbols (○, ◇, Δ) indicate the membrane region between the tenth carbons in each membrane leaflet (measurements with 10-, 12-, 14-, and 16-PC). P'_M(EPR) values for lens lipids and POPC/Chol were estimated with accuracies of ≪30% while for POPC with the accuracy of < 30% (see Section 3.1 for more explanation).

Table 1

Activation Energy for the Translational Diffusion of Molecular Oxygen in Investigated Membranes Calculated at Different Depths in the Membrane for the Temperature Region 15 to 45°C[a].

	activation energy (kcal/mol)							
	T-PC	**5-PC**	**7-PC**	**9-sasl**	**10-PC**	**12-PC**	**14-PC**	**16-PC**
lens lipids	6.5	9.3	6.8	8.0	4.6	4.1	4.5	3.1
POPC/Chol	6.0	6.0	7.3	7.0	4.3	4.1	4.3	3.4
POPC	5	6.2	5.6	nd[b]	5.4	4.6	nd[b]	4.6

[a] Since the overall oxygen concentration in the fluid phase membrane (above the phase-transition temperature) is practically independent of temperature [84,85], and the shape of the membrane profiles of $W(x)$ is practically independent of temperature in the fluid phase [9,10,55,57], the temperature-dependence of $W(x)$ can be attributed to the translational diffusion rate of molecular oxygen in the membrane. Since the Arhenius plots of the oxygen transport parameter (the plots of log$W(x)$ vs reciprocal temperature) show linear dependence on the reciprocal temperature between 15°C and 45°C for all spin labels (data not shown), the activation energies for oxygen translational diffusion in the investigated membranes were evaluated from the slopes. For more details, see Ref. [10].

[b] nd = not determined.